Density Analysis of LTE-LAA Networks Coexisting With WiFi Sharing Multiple Unlicensed Channels

HAONAN HU [1], (Member, IEEE), **YUAN GAO** [2], **JILIANG ZHANG** [2], (Senior Member, IEEE),
XIAOLI CHU [2], (Senior Member, IEEE), **QIANBIN CHEN** [1], AND **JIE ZHANG** [2]

[1]School of Communication and Information Engineering, Chongqing University of Posts and Telecommunications, Chongqing 400065, China
[2]Department of Electronic and Electrical Engineering, The University of Sheffield, Sheffield S1 3JD, U.K.

Corresponding author: Jiliang Zhang (jiliang.zhang@sheffield.ac.uk)

ABSTRACT With data traffic explosion, operating Long-Term Evolution (LTE) in the 5 GHz unlicensed band, which has already been used by WiFi networks, has been proposed. To harmoniously coexist with the incumbent WiFi networks, LTE-Licensed Assisted Access (LAA) has been proposed recently, advocating cellular networks to access the unlicensed band by employing listen-before-talk mechanism. However, the performance of LAA has not been analysed under multiple accessible unlicensed channels (UCs). In this work, we analyse the user throughput and spatial spectral efficiency (SSE) of the multi-UC coexisting LTE-LAA and WiFi networks versus the network density based on the Matern hard core process. The throughput and SSE are obtained as functions of the downlink successful transmission probability (STP), of which analytical expressions are derived and validated by Monte Carlo simulations. The results show that an optimal LTE access point (LAP) density exists to maximise the LTE-LAA user equipment (LUE) throughput, and our derived closed-form STP lower bound of LUE can be used to obtain a sufficiently accurate prediction of the optimal LAP density. Moreover, the SSE does not change much under relatively low LAP densities, and when the LAP density is larger than 1, 585 LAPs per km^2, the SSE approaches the asymptotic SSE as the LAP density approaches infinity.

INDEX TERMS LTE-LAA, WiFi, multiple unlicensed channels, Matern hard core process, successful transmission probability.

I. INTRODUCTION

With the proliferation of smart devices, a diversity of applications have been developed to fulfil user requirements supported by data transmissions in cellular networks. As a result, network traffic is growing at a precipitous rate. According to the prediction by Cisco [1], the total network traffic will reach 3.3 Zettabyte annually by 2021. This trend stimulates a requirement of $1000\times$ capacity increase in the forthcoming 5G networks. Due to the development of carrier aggregation technologies, the utilization of unlicensed spectrum bands has become a promising technique to achieve capacity enhancement in celllular networks [2].

In Releases 10-12 of the 3rd Generation Partnership Project (3GPP) standards [3], the Long Term Evolution

(LTE)-Unlicensed (LTE-U) scheme was introduced, encouraging LTE access points (APs) to access the 5 Gigahertz (GHz) unlicensed band, which has already been used by WiFi networks. The LTE-U scheme can potentially improve the spectral efficiency (SE) of the WiFi only network due to two aspects: 1) The spatial spectral effieciency can be increased by deploying LTE-U in LTE APs, especially under a low density of WiFi APs (WAPs); 2) Collisions in accessing the unlicensed band among users, which occur in WiFi networks because of the contention-based medium access contol (MAC) protocol among users, can be avoided by LTE-U via a centralized radio-resource-management protocol [4]. Furthermore, it has been shown that LTE-U APs can be good neighbours to WAPs if they deploy the carrier sensing adaptive transmission (CSAT) scheme [5], where adaptive duty cycles are used by LTE-U APs to leave certain time slots that only allow WAPs to access the unlicensed band. The 3GPP

Release 13 standardised the LTE-Licensed Assisted Access (LAA), which adheres to the requirement of listen before talk (LBT) mechanism in the LTE-LAA APs (LAPs). The LTE-LAA has been mainly defined for the downlink, and was extended to the uplink in the enhanced-LAA in 3GPP Release 14 [6]. New Radio Unlicensed (NR-U) has been investigated in the standards of 3GPP Release 16, which aims to operate the 5G NR in the unlicensed band with fair coexistence across different radio access technologies. Currently NR-U is working on five scenarios: a) carrier aggregation between licensed band NR and NR-U; b) dual connectivity between licensed band LTE and NR-U; c) stand-alone NR-U; d) an NR cell with downlink in unlicensed band and uplink in licensed band; e) dual connectivity between licensed band NR and NR-U [7]. LAA has been considered as a main operating mode in NR-U to enable operators to boost network capacity, which can be deployed in all the scenarios except the stand-alone one. Therefore, the investigation of the LAA performance in the LTE network coexisting with WiFi is still crucial and can provide insights for the future 5G NR-U deployment.

A. RELATED WORKS AND MOTIVATION

The performance of an LTE-U/LAA network coexisting with a WiFi network has been investigated in the literature. In [8], the user throughput and satisfaction of coexisting LTE-LAA and WiFi networks (CLWNets) were analysed. User satisfaction was defined as the channel utilization time per user. The LAPs adopt an LBT-based channel access scheme with adaptive channel sensing and usage times. The results showed that the CLWNets outperform the WiFi only network in terms of the average satisfaction of users by traffic offloading between licensed and unlicensed bands. In [9], the fairness between the LTE-U/LAA and WiFi networks in coexistence via the CSAT and LBT mechanisms were analysed, where the LBT mechanism adopted the carrier sense multiple access with collision avoidance (CSMA/CA) protocol. The results indicated that for short-time transmissions, the LBT mechanism can provide a better level of fairness, and for long-time transmissions, the levels of fairness provided by both schemes are identical. In [10], the fairness between the LTE-LAA and WiFi networks in coexistence via a fair LBT algorithm was analysed. The fair LBT algorithm was achieved by adjusting the idle period length in the frame-based LBT mechanism. The results indicated that this algorithm can improve the fairness while ensuring decent network sum throughput. In [11], the number of successful transmitted UEs is analysed in the CLWNets. The LAPs adopt a user-grouping based random access protocol with dynamic window size to avoid collisions. The results show that this protocol outperforms other baseline protocols in LTE-LAA. However, no analytical results were provided by these works.

Based on Markov chain model, the performance of the CLWNets in terms of transmission probability, throughput and channel access delay [12]–[15] have been studied analytically. In [12], the transmission probabilities of WAPs and LAPs in the CLWNets were analysed. The results indicated

that LAPs has a higher transmission probability as compared to WAPs. In [13], the expected network throughput of the CLWNets considering the frame structure and the back-off time was analysed and validated by Monte Carlo simulation. In [14], the throughput of the LTE-LAA networks with imperfect spectrum sensing was analysed based on the discrete-time Markov chain model. The results confirmed that the throughput was significantly affected by the imperfect spectrum sensing, and the throughput can be improved by jointly optimizing the sensing duration and sensing threshold. In [15], the average throughput and the channel access delay, caused by asymmetric hidden terminals, were analysed in CLWNets based on a joint Markov chain model. The results revealed that to achieve fairness in terms of the throughput, the lowest channel access priority of LTE-LAA was preferred. Nevertheless, the results based on Markov chain are valid for the small-scale CLWNets, which only conisder a single WAP or LAP with limited number of neighbouring LAPs or WAPs. For the large-scale CLWNets, in [16], based on stochastic geometry, the density of successful transmissions and rate coverage probability were analysed in coexisting LTE-U/LTE-LAA and WiFi networks under three mechanism (i.e., continuous transmission, CSAT, and LBT adopting CSMA/CA protocol) deployed in LTE APs. The results showed that the LTE-LAA scheme with the LBT can provide the best rate coverage probability. In [17], the fairness between the LTE-U and WiFi networks based on CSAT was analysed based on stochastic geometry, and the results revealed that a satisfactory level of fairness can be achieved by adjusting the duty cycle.

All the above mentioned works considered only a single unlicensed channel (UC), ignoring the general cases with multiple UCs. In [18], the average throughput achieved by an LTE AP or a WiFi AP, with the availability of multiple UCs, was evaluated by Monte Carlo simulation. The results showed that the fairness between LTE-U/LAA and WiFi networks can be maintained through UC selection. In [19], the collision probabilities between LAPs and WAPs were analysed under multiple accessible UCs. The results showed that LAPs' accesses to the UCs should be adapted to the WiFi traffic to guarantee a fair coexistence. In [20], the fairness of CLWNets was also analysed with multiple accessible UCs, and it was again concluded that the fairness can be achieved through UC selection and frame scheduling. In [21], the energy efficiency was analysed in the multi-UC CLWNets. The results showed that the optimal energy efficiency can be achieved by spectrum and power allocation. The coverage probability and throughput of a typical user, which has an equal probability being an LTE user or a WiFi user, were investigated in [22] under a multi-UC scenario. The results in [22] indicated that the coverage probability of a user increases with the number of accessible UCs. The fairness between the LTE-U and WiFi networks with multiple UCs was also analysed based on game theory in [23], and the fairness among UEs was analysed in a LTE-U driven multi-UC vehicle-to-everything and full-duplex assisted scenarios in [24] and [25], respectively.

To the best of our knowledge, the performance of large-scale CLWNets with multiple UCs has been analysed only in [22], where both LAPs and WAPs accessed UCs via the CSMA protocol, ignoring collision avoidance. However, the WAPs adopt the CSMA/CA protocol and the existing LBT mechanisms adopted by LAPs are fundamentally similar as the CSMA/CA protocol [6]. By using the CSMA/CA protocol, APs around the serving AP are no longer interference sources as the APs in this region will sense the carrier busy and keep silent, which is also ignored in [22]. Consequently, the performance of large-scale CLWNets both deploying the CSMA/CA protocol to access multiple UCs has not been sufficiently studied. Additionally, the technique in existing works (i.e., [16] and [17]) for the single-UC CLWNets using the CSMA/CA protocol is difficult to be extended into the multi-UC scenario. This is because in the single-UC scenario, if the typical AP has access to the UC, no APs having a back-off timer shorter than that of the typical AP are retained in its sensing region. As a result, it is unnecessary to consider the exact number of neighbouring APs of this typical AP (i.e., the interfering APs in its sensing region) to obtain its medium access probability (MAP). The MAP is defined as the probability of a typical AP being granted transmission. Nevertheless, in the multi-UC case, the typical AP can be retained in one of the UCs even if it does not have the shortest back-off timer among its neighbouring APs. Moreover, in the existing literature, the effects of the LAP density on the UE throughput and on the spatial spectrum efficiency (SSE) have not been studied in the CLWNets with multiple UCs.

In this work, by assuming LTE-LAA and WiFi networks both adopt CSMA/CA protocol [16], we investigate the large-scale coexisting LTE-LAA and WiFi networks sharing multiple UCs, and analyse the effects of LAP density on the above mentioned performance metrics numerically. Additionally, the fairness between the LTE-LAA and WiFi networks as a function of the LAP's sensing region radius is analysed. Furthermore, the asymptotic SSE as the LAP density approaches infinity is derived and is validated by simulations.

B. CONTRIBUTION

We are the first to provide performance analysis for a large-scale heterogeneous network (HetNet) comprising LAPs and WAPs that share multiple UCs both using the CSMA/CA protocol. The main contributions of this work are summarized as follows:

a) We obtain the MAPs of both LAPs and WAPs using the CSMA/CA protocol in a large-scale multi-UC CLWNets based on stochastic geometry. These MAPs are obtained in closed form and validated by Monte Carlo simulations. Based on the closed-from MAPs, analytical expressions of the downlink successful transmission probabilities (STPs), which are jointly determined by the downlink coverage probability of user equipment (UE) and the MAP of the serving AP, are derived and validated for both LTE-LAA UE (LUE) and WiFi UE (WUE).

b) To analyse the the effect of the LAP density on the UE throughput and the SSE of the CLWNets, we derive the analytical throughput and SSE expressions for both LUE and WUE, based on the validated STPs. The throughput expressions are then used to analyse the influence of the sensing-region radius of an LAP on the fairness of the CLWNets. Furthermore, the asymptotic SSE as the LAP density approaches infinity is derived and validated.

c) According to our analysis, firstly, there exists an optimal LAP density to maximize the LUE throughput. Our derived closed-form STP lower bound (LB) of LUE can be used to obtain a sufficiently accurate prediction of the optimal LAP density. Secondly, it is found that the SSE does not change much when the LAP density is relatively low, and that when the LAP density is over 1, 585 LAPs per km^2 (with an inter site distance of approximate 15 meters), the value of CLWNets SSE approaches the asymptotic SSE. Thirdly, with the optimal LAP density to maximise the LUE throughput, the more number of actively accessible UCs are preferable because the SSE becomes more close to the asymptotic SSE. Last but not the least, our analysis shows that the fairness between the LTE-LAA and WiFi networks can be achieved by adjusting the radius of an LAP's sensing region.

C. ORGANIZATION

The rest of this paper is organised as follows: Section II introduces the system model, including the network spatial distribution, propagation model, medium access scheme and defined performance metrics (i.e., STP, UE throughput, SSE). In this section, the closed-form MAPs are also derived and validated. Section III gives analytical results of the defined performance metrics, and we validate the analytical STPs by the Monte Carlo simulation. Only the STPs are validated because other performance metrics (i.e., UE throughput and SSE) are derived based on the STPs. Section IV presents the numerical analysis before concluding the paper in Section V.

Notations: Throughout the paper, we use $\mathbb{E}[\mathbf{X}]$ to denote the expectation of a random variable $\mathbf{X}$, $\mathbb{P}(Y)$ to denote the probability of an event Y, and $\mathcal{L}_{\mathbf{X}}(s)$ to denote the Laplace transform of a random variable $\mathbf{X}$ with parameter s.

II. SYSTEM MODEL

We consider a two-tier HetNet consisting of LAPs and WAPs, where LAPs form tier-L and WAPs form tier-W. LAPs and WAPs may vary in terms of density (λ_L and λ_W), sensing threshold (γ_L and γ_W), and transmit power (P_L and P_W). We assume that each AP in both tiers transmits in a full buffer mode, i.e., each AP always has data to transmit. We also assume perfect time synchronization throughout the two-tier HetNet. In the following subsections, the spatial locations of APs and UEs, the radio propagation model, the medium access scheme, and our defined performance metrics will be introduced. The symbols used in this paper are summarised in Table 1 together with their definitions and values used in simulations where applicable.

Symbol	Definition
Φ_L, Φ_W	Spatial PPPs of LAPs and WAPs
λ_L, λ_W	Densities of LAPs and WAPs
P_L, P_W	Transmission powers of LAPs and WAPs
Λ_c	Wavelength of carrier frequency
α	Pathloss exponent
M	Non-overlapping channel number
μ	Rayleigh fading parameter
σ^2	Thermal noise power
γ_L, γ_W	Sensing signal strength thresholds of LAPs and WAPs
κ_L	LAP sensing region factor
R_L, R_W	Sensing radiuses of LAPs and WAPs
T, B	SINR threshold, Bandwidth per channel
$t_\mathbf{x}, t_\mathbf{y}$	Back-off timers of LAPs and WAPs
$e_\mathbf{x}^L, e_\mathbf{y}^W$	Medium access indicators of LAPs and WAPs
$\tilde{\Phi}_L, \tilde{\Phi}_W$	Retained interfering LAPs and WAPs
$\tilde{e}_\mathbf{x}^{LL}, \tilde{e}_\mathbf{y}^{LW}$ $(\tilde{e}_\mathbf{x}^{WL}, \tilde{e}_\mathbf{y}^{WW})$	Modified retaining indicators of interfering LAPs and WAPs for a tagged LAP (WAP)
ξ	Tier-ξ AP is LAP if $\xi = L$ and WAP if $\xi = W$
h_i^{LL}, h_j^{LW} (h_i^{WL}, h_j^{WW})	Fading of the channel from the LAP $\mathbf{x}_i$ and the WAP $\mathbf{y}_j$ to the LAP (WAP) user
$\mathcal{B}(\mathbf{z}, r)$	Open ball with center $\mathbf{z}$ and radius r
$\mathcal{B}^c(\mathbf{z}, r)$	Complement of $\mathcal{B}(\mathbf{z}, r)$

A. SPATIAL LOCATIONS

The LAPs and WAPs are distributed following two independent Poisson point processes (PPPs) [26], denoted by $\Phi_L = \{\mathbf{x}_1, \mathbf{x}_2, \cdots \mathbf{x}_i, \cdots\}$ and $\Phi_W = \{\mathbf{y}_1, \mathbf{y}_2, \cdots \mathbf{y}_j, \cdots\}$ with densities λ_L and λ_W, respectively. For analytical tractability, we assume that there are two independent groups of UEs, i.e., LUEs that each served by its closest LAP, and WUEs that each served by its closest WAP. A user association scheme across LTE-LAA and WiFi networks is out of the scope of this work. LUEs and WUEs are distributed following two independent PPPs, with densities much larger than those of LAPs and WAPs. Thus, we can assume that each AP has at least one associated UE [16].

B. PROPAGATION MODEL

We assume that each link between a UE and an AP experiences pathloss and small scale fading. The shadowing is neglected to ensure analytical tractability [27]. The pathloss follows a log-distance model given in decibels (dB) as $l(d) = 20 \log_{10}(\frac{4\pi}{\Lambda_c}) + 10\alpha \log_{10}(d)$, where d is the distance between the transmitter and receiver, Λ_c is the wavelength, and α is the pathloss exponent ($2 < \alpha \leq 6$) [28]. For the small scale fading, Rayleigh fading is assumed, thus the received power attenuation caused by it is modelled as an independent exponential distribution with a rate parameter μ. Specifically, the small scale fading of the link between an LAP $\mathbf{x}_i$ or a WAP $\mathbf{y}_j$ and a typical LUE (WUE) is denoted by h_i^{LL} or h_i^{WL} (h_i^{LW} or h_i^{WW}), respectively.

C. MEDIUM ACCESS SCHEME WITH MULTIPLE UCS

According to the IEEE 802.11 a/n/ac, the 5 GHz unlicensed bands, i.e., $5.15 - 5.35$ GHz and $5.47 - 5.825$ GHz, is divided into a number of UCs, each with a bandwidth of 20, 40, 80, or 160 MHz [29]. Since a maximum of 100 MHz bandwidth

in the licensed or unlicensed bands can be supported by carrier aggregation [30], we assume that the entire 5 GHz unlicensed band is divided into M non-overlapping UCs [22], and there is no mutual interference between any two different UCs. The maximum number of UCs M is influenced by the bandwidth of an UC. In the 5 GHz unlicensed band with an approximate total bandwidth of 490 MHz, a maximum of 24 non-overlapping UCs, each with a bandwidth of 20 MHz, can be supported [29].

As the LBT-based medium access scheme is deployed in LAPs, we assume that both WAPs and LAPs adopt CSMA/CA protocol to access the M UCs. According to [31], the LBT scheme can be mainly categorised into the frame-based LBT and the load-based LBT. The main difference between these two schemes is that the size of contention window (CW) of the frame-based LBT is fixed while that of the load-based LBT is random. In this work, we employ the load-based LBT, the mechanism of which is fundamentally similar to the CSMA/CA protocol [6], where the minimum and the maximum CW sizes are 15 and 1023, respectively. The WAP randomly selects a number between 0 and the current CW size and counts down that number of idle slots, whose length is 9 μs each, before the transmission. For the load-based LBT, if the priority class is 1, then the minimum and maximum CW sizes are exactly the same as those of the CSMA/CA protocol, and the slot duration is at least 9 μs, which is the same as a WiFi slot [29]. Additionally, the exponential increase in the back-off CW size has been adopted in both the CSMA/CA protocol and the load-based LBT [32]. Therefore, if the slot duration of the load-based LBT is 9 μs, we can assume that both the LAPs and WAPs use the CSMA/CA protocol. The other priority classes (i.e., 2-4) of the load-based LBT have either a smaller minimum CW size or a smaller maximum CW size. As a result, for priority classes 2-4, the MAP of an LAP is larger while the MAP of a WAP is smaller than those obtained in our work, respectively.

The sensing thresholds in the CSMA/CA protocol used by LAPs and WAPs are denoted by γ_L and γ_W, respectively, which determine their sensing regions. For analytical tractability of the MAP for each AP, we ignore the effect of small scale fading on the sensing regions [18], [22], [33]–[35], thus the radius R_W of the sensing region of a WAP is given by $R_W = \left(\frac{P_W \Lambda_c^2}{\gamma_W (4\pi)^2}\right)^{\frac{1}{\alpha}}$. Since the differences between the carrier frequencies in different UCs in the 5 GHz unlicensed band are much smaller than 5 GHz, we use 5 GHz as the approximate common carrier frequency for all the M UCs. As a result, the wavelength Λ_c is 0.06 m. Similar as the WAP, the radius R_L of the sensing region of an LAP is given by $R_L = \left(\frac{P_L \Lambda_c^2}{\gamma_L (4\pi)^2}\right)^{\frac{1}{\alpha}}$. By defining $\kappa_L = \frac{R_L}{R_W}$ as the LAP sensing region factor, we have $R_L = \kappa_L R_W$. The spatial locations and the sensing radiuses of LAPs and WAPs are illustrated in Fig. 1. Moreover, we assume that each LAP and WAP can detect all the idle UCs, and will randomly access one of them if there are multiple idle UCs [36].
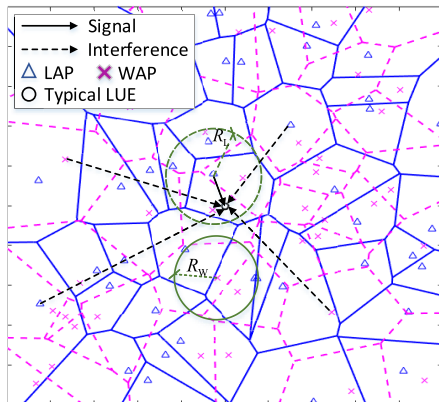
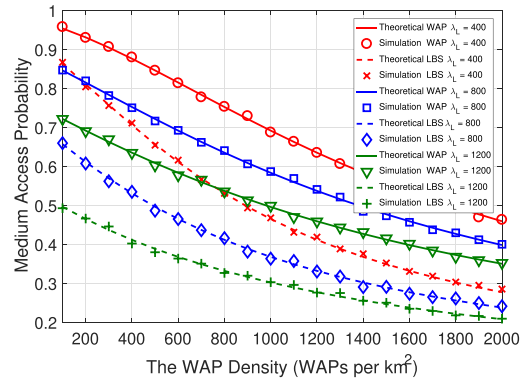**FIGURE 1.** Illustration of the system model with a typical LUE.

FIGURE 2. The MAP validation versus the WAP density with $P_L = P_W = 23$ dBm, $\alpha = 4$, $M = 3$, $\mu = 1$, $\gamma_W = -82$ dBm.

If APs start to transmit instantly after detecting an idle UC, collisions between simultaneous data transmissions on the same channel from several APs may occur. In order to reduce such collisions, a back-off timer, which is independently and uniformly distributed in the range of [0, 1] [16], [17], is employed at each AP in both tiers. The back-off timer decides the time period that the AP should wait before transmission on an idle UC. The back-off timers are respectively denoted by $\{t_{\mathbf{x}_1}, t_{\mathbf{x}_2}, \cdots, t_{\mathbf{x}_i}, \cdots\}$ and $\{t_{\mathbf{y}_1}, t_{\mathbf{y}_3}, \cdots, t_{\mathbf{y}_j}, \cdots\}$ for LAPs and WAPs. Although the simple uniform distribution of the back-off timer ignores its exponentially increasing characteristic related to the collision time, it can still provide reasonable results in modeling the CSMA/CA protocol [37], which grants access of an idle channel to the AP with the minimum back-off timer. Accordingly, the medium access scheme for APs in both tiers can be described as follows: For a specific AP, its neighbouring APs are defined as the set of WAPs and LAPs in its sensing region. If the number of neighbouring APs is smaller than the UC number M, then this specific AP will be granted transmission, as there is at least one available UC to access. Otherwise, this AP will be granted transmission on an idle UC only if its back-off timer is among the lowest M ones of all the neighbouring APs. A medium access indicator, which is configured as 1 if the AP is granted transmission and as 0 otherwise, is assigned to each AP. A transmission-granted AP is also namely as a retained AP. The medium access indicators of the i-th tier-ξ AP ($\xi \in \{L, W\}$), denoted by $e_{\mathbf{z}_i}^{\xi}$, can be given as below:

$$e_{\mathbf{z}_i}^{\xi} = \mathbf{1}_{(\mathcal{N}_{\mathbf{z}_i}(R_\xi) < M)} + \mathbf{1}_{(\mathcal{N}_{\mathbf{z}_i}(R_\xi) \geq M)(t_{\mathbf{z}_i} < \Delta(\mathcal{T}_{\mathbf{z}_i}(R_\xi)), M)}, \quad (1)$$

where $\mathbf{z} = \mathbf{x}$ if $\xi = L$ and otherwise $\mathbf{z} = \mathbf{y}$, $\mathcal{N}_{\mathbf{z}_i}(\epsilon)$ and $\mathcal{T}_{\mathbf{z}_i}(\epsilon)$ denote the number and the set of back-off timers of neighbouring APs around a typical AP locating at $\mathbf{z}_i$ with a sensing region radius ϵ, respectively. The function $\Delta(\mathbf{S}, n)$ returns the n-th smallest element in set $\mathbf{S}$. Accordingly, the MAP, which

is defined as the probability of a typical AP being granted transmission, is given in Lemma 1.

Lemma 1: Assuming that LAPs and WAPs have the same channel access priority, and each AP can detect the transmitting behaviours of all other APs in its sensing region with radius R_ξ, the MAP ϑ_ξ of a tier-ξ AP located at the origin is given by $\vartheta_\xi = \mathcal{A}(N_{o,\xi}, M)$, where $\xi \in \{L, W\}$. The tier-ξ AP is an LAP if $\xi = L$ and is a WAP if $\xi = W$. $N_{o,\xi}$ is the expected number of neighbouring APs in the sensing region of $\mathcal{B}_o(R_\xi)$, in which o denotes the origin and $\mathcal{B}_{\mathbf{z}}(\epsilon)$ denotes a two-dimensional open ball centred at $\mathbf{z}$ with a sensing radius ϵ. The function $\mathcal{A}(a, b)$ is defined in (2), as shown at the bottom of this page, where a and b are two arbitrary parameters, and the term $\Gamma(\widehat{b}, a)$ is the upper incomplete Gamma function, defined as $\Gamma(\widehat{b}, a) = \int_a^\infty u^{\widehat{b}-1} e^{-u} du$ with $\widehat{b} = b + 1$ or $b + 2$.

Proof: See Appendix A.

Fig. 2 illustrates the theoretical and Monte-Carlo simulated MAPs of a typical LAP and a typical WAP versus the WAP density under three different LAP densities: 400, 800 and 1200 LAPs per km². Each simulation curve is obtained by averaging over 10, 000 realizations of LAP and WAP locations following two independent PPPs in a square area of 25 km², where the typical LAP or WAP is located at the origin. The theoretical curves are obtained following Lemma 1. The results show that the theoretical MAPs closely match the simulation results for both tiers of APs. This verifies the accuracy of our derived MAP expression. In addition, we can see that the MAP of the typical LAP is lower than that of the WAP, because the sensing region of an LAP is larger than that of a WAP ($\kappa_L = 1.3$).

The steps of the Monte Carlo simulation to obtain the MAP are summarized as follows:

Step 1: In each realization, the positions of LAPs and WAPs are modelled following two independent PPPs in a square range of 25 km², and a typical LAP or WAP is located at the origin.

$$\mathcal{A}(a, b) = \frac{1}{a}\left[b + \frac{\Gamma(b+1, a)}{\Gamma(b+1, 0)} + (a - 1 - b)\frac{\Gamma(b+2, a)}{\Gamma(b+2, 0)} - e^{-a}\frac{a^{b+1}}{\Gamma(b+2, 0)} \right] \quad (2)$$

Step 2: Each LAP or WAP is allocated with a back-off timer following independent uniform distribution in the range of [0, 1].

Step 3: The medium access status of the typical LAP or WAP is simulated following equation (1). If the typical LAP or WAP is retained, the medium access status equals 1, and otherwise, the medium access status equals 0.

Step 4: We run 10,000 realizations of the above-mentioned steps. We obtain the MAP via dividing the times of medium access status being 1 by the total realization times.

D. PERFORMANCE METRICS

In this work, we mainly analyse the STP and the throughput of both LUE and WUE, and the SSE of the CLWNets.

1) SUCCESSFUL TRANSMISSION PROBABILITY

The STP of a typical UE is defined as the probability of the typical UE simultaneously satisfying the following two conditions: a) Its serving AP is retained; b) Its SINR is larger than a threshold T_ξ. Denoting the medium access indicators and the SINR of the nearest tier-ξ AP as e_0^ξ and Ψ_0^ξ, respectively, the STPs of a typical tier-ξ UE is given as:

$$\mathcal{P}_{st}^\xi(\lambda_L, \lambda_W, T_\xi, M) = \mathbb{E}[e_0^\xi]\mathbb{P}(\Psi_0^\xi > T_\xi | e_0^\xi = 1). \quad (3)$$

As we assume that each LUE/WUE is associated to its nearest LAP/WAP, the desired signal of each LUE/WUE is from its nearest LAP/WAP, while the other retained APs are the sources of interference. Thus, the SINR expressions of the typical LUE and the typical WUE are respectively given as follows:

$$\Psi_0^L = \frac{P_L h_0^{LL} l_L(||\mathbf{x}_0||)}{I_{\widetilde\Phi_L/\mathbf{x}_0} + I_{\widetilde\Phi_W} + \sigma^2}, \quad \Psi_0^W = \frac{P_W h_0^{WW} l_W(||\mathbf{y}_0||)}{I_{\widetilde\Phi_W/\mathbf{y}_0} + I_{\widetilde\Phi_L} + \sigma^2}, \quad (4)$$

where $I_{\widetilde\Phi_L} = \sum_{\mathbf{x}_i \in \widetilde\Phi_L} P_L h_i^{WL} l_L(||\mathbf{x}_i||)$ and $I_{\widetilde\Phi_L/\mathbf{x}_0} = \sum_{\mathbf{x}_i \in \widetilde\Phi_L/\mathbf{x}_0} P_L h_i^{LL} l_L(||\mathbf{x}_i||)$, $I_{\widetilde\Phi_W} = \sum_{\mathbf{y}_j \in \widetilde\Phi_W} P_W h_j^{LW} l_W(||\mathbf{y}_j||)$ and $I_{\widetilde\Phi_W/\mathbf{y}_0} = \sum_{\mathbf{y}_j \in \widetilde\Phi_W/\mathbf{y}_0} P_W h_j^{WW} l_W(||\mathbf{y}_j||)$. $\widetilde\Phi_W$ and $\widetilde\Phi_L$ respectively denote the retained interfering WAPs and LAPs which use the same channel as the serving AP, $||\varpi||$ is the Euclidean distance between the location ϖ and the origin, and σ^2 is the thermal noise.

2) UE THROUGHPUT

The UE throughput is defined as the throughput of a typical UE at a predefined SINR threshold [17], [33], [38], which can reduce the calculation complexity of the UE throughput. As the UE locations in the same tier follow a homogeneous PPP, the throughputs of contending UEs associated with the same AP follow the same distribution. Thus without loss of generality, we assume the typical UE is allocated with all the radio resources. The UE throughput can be considered as the aggregate throughput of associated UEs for an AP. Note that when the serving AP of this typical UE is not retained, i.e., the

serving AP is not granted transmission on any UC, the UE throughput equals 0. As aforementioned, each AP in both tiers can access only one of the idle UCs, thus the throughput of a tier-ξ UE is given by:

$$\mathcal{C}_\xi(\lambda_L, \lambda_W, T_\xi, M) = \mathbb{E}[e_0^\xi] B \log(1+T_\xi)\mathbb{P}(\Psi_0^\xi > T_\xi | e_0^\xi = 1), \quad (5)$$

where B is the bandwidth per UC.

3) SPATIAL SPECTRAL EFFICIENCY

We define the SSE as the aggregate throughput provided by the retained APs of both tiers in a unit square area per Hz, which can be expressed as:

$$\Theta = \frac{1}{MB} \sum_{\xi \in \{L, W\}} \lambda_\xi \mathcal{C}_\xi(\lambda_L, \lambda_W, T_\xi, M). \quad (6)$$

III. PERFORMANCE ANALYSIS

In this section, firstly we derive the MAP of the serving AP and the Palm coverage probability [39] to obtain the STP. Secondly, the UE throughput and the SSE are analysed based on the STP. Without loss of generality, we place the typical UE at the origin, which is justified by the Slivnyak's theorem [27] since the LUEs and the WUEs are distributed following two independent homogeneous PPPs.

A. THE MAP OF THE SERVING AP

The MAP of the serving AP of the typical UE differs from that of a typical AP because it considers the distance between the typical UE and its serving AP. Note that each LUE and each WUE is served by its closest LAP and WAP, respectively. As a result, the distances between the typical UE and other APs, which are in the same tier as the serving AP, must be larger than that between the typical UE and the serving AP. Denoting the position of the serving AP by $(r_0^\xi, 0)$, where r_0^ξ is the distance between the serving LAP and the typical LUE if $\xi = L$, and is the distance between the serving WAP and the typical WUE otherwise, $\xi \in \{L, W\}$. Conditioned on this, the MAP of the serving AP is given in Lemma 2.

Lemma 2: For a tier-ξ serving AP $\mathbf{z}_0^\xi$ located at $(r_0^\xi, 0)$ with M accessible UCs, its MAP is given by:

$$\mathbb{P}(e_0^\xi = 1 | \mathbf{z}_0^\xi = (r_0^\xi, 0)) = \mathcal{A}(N_{o,\xi} - \lambda_\xi \mathcal{V}_{int}(r_0^\xi, R_\xi, r_0^\xi), M), \quad (7)$$

where $\xi \in \{L, W\}$, R_ξ is the sensing radius of the tier-ξ AP, and the function $\mathcal{V}_{int}(r_m, r_n, d)$ denotes the intersection area of two circles, where r_m and r_n are the radius of the two circles and d is the distance between the centres of the two circles. $\mathcal{V}_{int}(r_m, r_n, d)$ equals $\pi(\min(r_m, r_n))^2$ if $d \leq \max(r_m, r_n) - \min(r_m, r_n)$, equals 0 if $d \geq r_m + r_n$ and otherwise equals $a^2(\beta_{r_m} - \sin 2\beta_{r_m}) + b^2(\beta_{r_n} - \sin 2\beta_{r_n})$, where $\beta_{r_m} = \arccos\left(\frac{r_m^2 + d^2 - r_n^2}{2r_m d}\right)$ and $\beta_{r_n} = \arccos\left(\frac{r_n^2 + d^2 - r_m^2}{2r_n d}\right)$.

Proof: See Appendix B.

Based on the PDF of the closest tier-ξ AP [27], i.e., $f_{r_0^\xi}(r) = 2\pi\lambda_\xi r \exp(-\pi\lambda_\xi r^2)$, the MAP of the serving tier-ξ AP can be calculated by (8), as shown at the bottom of this page.

B. THE PALM COVERAGE PROBABILITY

The Palm coverage probability is defined as the probability of the SINR of a typical tier-ξ UE being larger than a threshold T_ξ, conditioned on the known location of the serving AP. For a tier-ξ serving AP $\mathbf{z}_0^\xi$ locating at $(r_0^\xi, 0)$, the Palm coverage probability of the typical UE is denoted by $\mathbb{P}_{\mathbf{z}_0^\xi}(\Psi_0^\xi > T_\xi | e_0^\xi = 1, \mathbf{z}_0 = (r_0^\xi, 0))$, which can be transformed as follows:

$$\mathbb{P}_{\mathbf{z}_0^\xi}(\Psi_0^\xi > T_\xi | e_0^\xi = 1, \mathbf{z}_0 = (r_0^\xi, 0)) \tag{9}$$

$$= \mathbb{P}(\Psi_0^\xi > T_\xi | \mathbf{z}_0 = (r_0^\xi, 0), \Phi_\xi[B_o(r_0^\xi)] = 0, e_0^\xi = 1) \tag{10}$$

$$= \mathbb{P}\left(\frac{P_\xi h_0^{\xi L} l_\xi(||\mathbf{z}_0^\xi||)}{\widetilde{I}_{\xi L} + \widetilde{I}_{\xi W} + \sigma^2} > T_\xi | e_0^\xi = 1\right), \tag{11}$$

where $\widetilde{I}_{\xi L} = \sum_{\mathbf{x}_i \in \widetilde{\Phi}_{\xi L}/\mathbf{x}_0} P_L h_i^{\xi L} l_L(||\mathbf{x}_i||)$ and $\widetilde{I}_{\xi W} = \sum_{\mathbf{y}_j \in \widetilde{\Phi}_{\xi W}} P_W h_j^{\xi W} l_W(||\mathbf{y}_j||)$. Thus in order to obtain the Palm coverage probability, the distribution of the aggregate interference, i.e., $\widetilde{I}_{\xi L}$ and $\widetilde{I}_{\xi W}$, should be derived first. According to [39], the retained interfering LAPs and WAPs form a Matern hard core process (MHCP), but the closed-form Laplace transformation of the aggregate interference power based on an MHCP is still unknown. Fortunately, an approximation method, which treats the MHCP as an independent inhomogeneous thinning process by decoupling the thinning dependence between the interfering APs, has been proven effective for performance analysis in [16], [17], [22], [40]. Based on the approximation method, the retaining probability of an interfering AP correlates only with the transmission state of the serving AP. Accordingly, we give the retaining probability of an interfering LAP/WAP conditioned on a location-known serving tier-ξ AP being retained as below.

Proposition 1: Conditioned on the serving tier-ξ AP $\mathbf{z}_0^\xi$ transmitting at $(r_0^\xi, 0)$, the retaining probabilities of an interfering LAP $\mathbf{x}_i$ and WAP $\mathbf{y}_j$ are respectively given as follows:

$$\mathcal{R}_{\xi L}(\mathbf{x}_i) \approx \begin{cases} \mathcal{A}(N_{\mathbf{x}_i, L}, M)/M, & \mathbf{x}_i \in V_0^\xi(L) \cap V_1^\xi(L), \\ \mathcal{A}(N_{\mathbf{x}_i, L}^*, M)/M, & \mathbf{x}_i \in V_0^\xi(L) \cap V_2^\xi(L), \\ 0, & Otherwise, \end{cases} \tag{12}$$

$$\mathcal{R}_{\xi W}(\mathbf{y}_j) \approx \begin{cases} \mathcal{A}(N_{\mathbf{y}_j, W}, M)/M, & \mathbf{y}_j \in V_0^\xi(W) \cap V_1^\xi(W), \\ \mathcal{A}(N_{\mathbf{y}_j, W}^*, M)/M, & \mathbf{y}_j \in V_0^\xi(W) \cap V_2^\xi(W), \\ 0, & Otherwise, \end{cases} \tag{13}$$

where $N_{\mathbf{x}_i, L}^*$ and $N_{\mathbf{y}_j, W}^*$ equals $N_{\mathbf{x}_i, L} - \lambda_\xi \mathcal{V}_{int}(R_L, r_0^\xi, ||\mathbf{x}_i||)$ and $N_{\mathbf{y}_j, W} - \lambda_\xi \mathcal{V}_{int}(R_W, r_0^\xi, ||\mathbf{y}_j||)$, respectively. $V_0^\xi(\widehat{\xi}) = \mathcal{B}^c(\mathbf{z}_0^\xi, \max\{R_{\widehat{\xi}}, R_\xi\})$, $V_1^\xi(\widehat{\xi}) = \mathcal{B}(o, r_0^\xi + R_{\widehat{\xi}})$, and $V_2^\xi(\widehat{\xi}) = \mathcal{B}(o, r_0^\xi + R_{\widehat{\xi}})$, if $\xi = \widehat{\xi}$, otherwise, $V_2^\xi(\widehat{\xi}) = \mathcal{B}(o, r_0^\xi + R_{\widehat{\xi}}) \cap \mathcal{B}^c(o, r_0^\xi)$, $\widehat{\xi} \in \{L, W\}$. Note that both $\mathcal{R}_{\xi L}(\mathbf{x}_i)$ and $\mathcal{R}_{\xi W}(\mathbf{y}_j)$ are related to λ_W, λ_L, and M, which are neglected in the notation for simplicity.

Proof: See Appendix C.

Equipped with the retaining probabilities of the two-tier interfering APs, the Palm coverage probabilities of the LTE-LAA and the WiFi users are given in Lemma 3.

Lemma 3: In the CLWNets with M UCs and an SINR threshold of T_L, conditioned on the serving LAP $\mathbf{x}_0$ located at $(r_0^L, 0)$, the Palm coverage probability of the LUE, denoted by $p_{\mathbf{x}_0}(r_0^L, \lambda_W, \lambda_L, T_L, M)$, can be approximately obtained as the expression in (14), as shown at the bottom of the next page. For the WUE, its Palm coverage probability $p_{\mathbf{y}_0}(r_0^W, \lambda_W, \lambda_L, T_W, M)$ can be approximately obtained as the expression in (15), as shown at the bottom of the next page conditioned on the serving WAP $\mathbf{y}_0$ located at $(r_0^W, 0)$. $\mathsf{p}(\rho, \theta)$ denotes a point in the Cartesian coordinate system with radius of ρ and angle of θ in the polar coordinate system, which translates the locations of retained interfering APs from the polar coordinate system into the Cartesian coordinate system, which can be expressed as $\mathsf{p}(\rho, \theta) = (\rho\cos(\theta), \rho\sin(\theta))$.

Proof: See Appendix D.

The Palm coverage probability can be utilised to obtain the coverage probability of a UE if the location of its serving AP is known. As the PDF of the distance between a UE and its serving AP has already been obtained in Section III-A, the coverage probability of a UE can be obtained by removing the condition on the serving AP location from the results in Lemma 3. The coverage probability is critical for the STP, which will be discussed in the next subsection.

C. THE STP, UE THROUGHPUT AND SSE

Recall that the STP of a typical UE is defined as the probability of the UE's SINR being larger than a threshold T while its serving AP being retained. Combining the results in (8) with those in Lemma 3, we present the STPs of the LUE and the WUE in Theorem 1.

Theorem 1: In the CLWNets with M UCs and an SINR threshold of T_ξ, the STPs of a tier-ξ UE, denoted by $\mathcal{P}_{st}^\xi$, can be approximated as:

$$\mathcal{P}_{st}^\xi \approx \mathbb{P}(e_0^\xi = 1) \int_0^\infty p_{\mathbf{z}_0^\xi}(r, \lambda_W, \lambda_L, T_\xi, M) f_{r_0^\xi}(r) dr, \tag{16}$$

where $\mathbf{z}_0^\xi$ equals $\mathbf{x}_0$ if $\xi = L$, and otherwise $\mathbf{z}_0^\xi = \mathbf{y}_0$.

Since the terms $\mathbb{P}(e_0^\xi = 1)$ and $p_{\mathbf{z}_0^\xi}(r, \lambda_W, \lambda_L, T_\xi, M)$ correlate with the function $\mathcal{A}(\cdot)$ given in (2), which contains

$$\mathbb{P}(e_0^\xi = 1) = \int_0^{\frac{R_\xi}{2}} \mathcal{A}(N_{o,\xi} - \lambda_\xi \pi r^2, M) 2\pi\lambda_\xi r e^{-\lambda_\xi \pi r^2} dr + \int_{\frac{R_\xi}{2}}^\infty \mathcal{A}(N_{o,\xi} - \lambda_\xi \mathcal{V}_{int}(r, R_\xi, r), M) 2\pi\lambda_\xi r e^{-\lambda_\xi \pi r^2} dr \tag{8}$$

TABLE 2. Simulation values.

| Parameter	Simulation Value	Parameter	Simulation Value
$P_L = P_W$	23 dBm	σ^2	0
$T_L = T_W$	5 dB	γ_W	−82 dBm
α	4	κ_L	1.3
M	3	Λ_c	0.06 m
μ	1	B	20 MHz

the upper incomplete Gamma function, closed-form results of the STPs are difficult to obtain. The STPs for both-tier UEs are validated through comparison with Monte Carlo simulation results, which are based on 10, 000 realizations of random locations of LAPs and WAPs with the typical LUE or WUE at the origin. In each realization, the closest LAP and WAP are selected as the serving AP for the LUE and the WUE, respectively, and the retaining status of all APs are determined according to our proposed medium access scheme in Section II-C. If the serving AP is not retained, then the SINR of the typical UE is set as 0. We assume that the retained LAPs and WAPs each independently have the probability of $1/M$ to access the same channel as the serving AP. The simulation parameters are listed in Table 2 unless otherwise specified.

The steps of the Monte Carlo simulation to obtain the STP are summarized as follows:

Step 1: In each realization, the positions of LAPs and WAPs are modeled following two independent PPPs in a square range of 25 km², and a typical LUE or WUE is located at the origin.

Step 2: Associate the typical LUE or WUE to its nearest LAP or WAP, meanwhile allocate a back-off timer to each LAP and WAP, and each back-off timer follows an identical independent uniform distribution in the range of [0, 1]. After this, judge the medium access status of the associated LAP or WAP based on equation (1).

Step 3: If the medium access status equals 1, go to Step 4. Otherwise, the transmission in this realization fails.

Step 4: The retained interfering LAPs and WAPs are simulated following equation (12). As a result, the SINR value of the typical LUE or WUE can be obtained.

Step 5: If the SINR is larger than the predefined threshold, the transmission in this realization succeeds. Otherwise, this transmission fails.
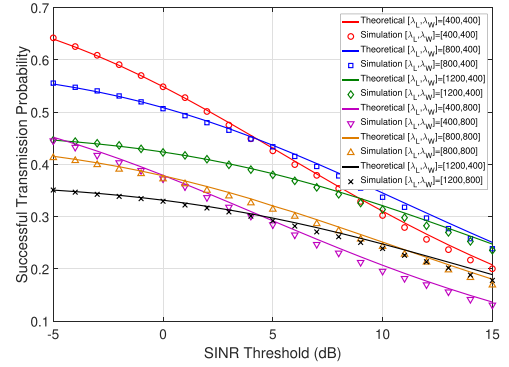
(a) The STP of the LUE
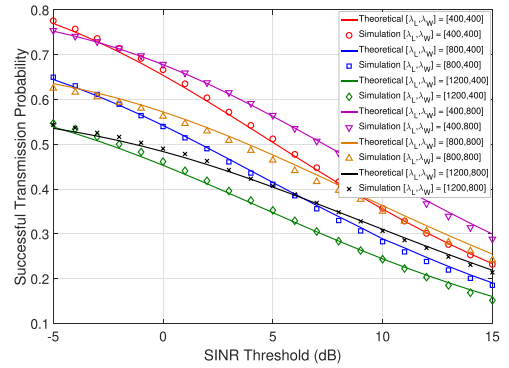
(b) The STP of the WUE

FIGURE 3. The validation of STPs versus the SINR threshold.

Step 6: We run 10,000 realizations of the above mentioned steps. We obtain the successful transmission probability via dividing the times of successful transmission by total realization times.

Fig. 3(a) and Fig. 3(b) respectively plot the theoretical and simulated STPs of a typical LUE and a typical WUE, versus the SINR threshold for $\lambda_L = \{400, 800, 1200\}$ LAPs per km² and $\lambda_W = \{400, 800\}$ WAPs per km². Firstly, the results show that the theoretical STPs closely match the simulated STPs, validating the accuracy of our analytical expressions of the STPs. Secondly, the STP of an LUE does not always increase with the LAP density. This is because the increased coverage probability, due to the shorter serving-LAP distance, cannot compensate for the decreased serving-LAP MAP for low to medium values of the SINR thresholds. Thirdly, the STP of a WUE degrades significantly with the increase of the

$$p_{\mathbf{x}_0}(r_0^L, \lambda_W, \lambda_L, T_L, M) \approx \exp\left(-\int_0^{2\pi}\int_{r_0^L}^{\infty}\frac{\lambda_L \mathcal{R}_{LL}(\mathsf{p}(\rho,\theta))}{1+\frac{l_L(r_0^L)}{T_L l_L(\rho)}}\rho d\rho d\theta - \int_0^{2\pi}\int_0^{\infty}\frac{\lambda_W \mathcal{R}_{LW}(\mathsf{p}(\rho,\theta))}{1+\frac{P_L l_L(r_0^L)}{P_W T_L l_W(\rho)}}\rho d\rho d\theta - \frac{\mu T_L \sigma^2}{P_L l_L(r_0^L)}\right)$$

$$(14)$$

$$p_{\mathbf{y}_0}(r_0^W, \lambda_W, \lambda_L, T_W, M) \approx \exp\left(-\int_0^{2\pi}\int_{r_0^W}^{\infty}\frac{\lambda_W \mathcal{R}_{WW}(\mathsf{p}(\rho,\theta))}{1+\frac{l_W(r_0^W)}{T_W l_W(\rho)}}\rho d\rho d\theta - \int_0^{2\pi}\int_0^{\infty}\frac{\lambda_L \mathcal{R}_{WL}(\mathsf{p}(\rho,\theta))}{1+\frac{P_W l_W(r_0^W)}{P_L T_W l_L(\rho)}}\rho d\rho d\theta - \frac{\mu T_W \sigma^2}{P_W l_W(r_0^W)}\right)$$

$$(15)$$

LAP density. This degradation can be reduced by deploying more WAPs in the network.

Based on the validated STPs, the tier-ξ UE throughput $\mathcal{C}_\xi(\lambda_L, \lambda_W, T_\xi, M)$, defined in (5), is given by $B\log(1 + T_\xi)\mathcal{P}_{st}^\xi$. The SSE Θ of the CLWNets can be obtained by combining the UE throughput expressions with (6). Consequently, the STPs and throughput of UEs, and the SSE of the CLWNets can be analysed numerically.

D. THE OPTIMAL LAP DENSITY

According to the results in Section IV, the optimal LAP density for maximising the LUE throughput exists. Therefore, in this subsection, we derive a closed-form STP LB of the LUE, which can be used to obtain a sufficiently accurate prediction of the optimal LAP density. By assuming the thermal noise power $\sigma^2 = 0$, the STP LB of the LUE is provided in Corollary 1.

Corollary 1: The STP LB $\widehat{\mathcal{P}}_{st}^L$ of the typical LUE is given as:

$$\widehat{\mathcal{P}}_{st}^L = \frac{M\vartheta_L}{M + T_L^{\frac{2}{\alpha}}\left[\mathcal{D}(\alpha, T_L) + \frac{\lambda_W}{\lambda_L}(\frac{P_W}{P_L})^{\frac{2}{\alpha}} sinc^{-1}(\frac{2\pi}{\alpha})\right]}, \quad (17)$$

where $\mathcal{D}(\alpha, T_L) = sinc^{-1}(\frac{2\pi}{\alpha}) - {}_2F^1(1, \frac{2}{\alpha}; 1 + \frac{2}{\alpha}; -\frac{1}{T_L})$.

Proof: See Appendix E.

By combining (17) with UE throughput expressions, we can obtain the approximate optimal LAP density λ_L^* for maximising the LUE throughput as the result in (18), as shown at the bottom of this page. Because the upper incomplete Gamma function occurs at the right hand side of (18), it is difficult to obtain the closed-form approximate optimal LAP density. As a result, we analyse this optimal LAP density numerically in Section IV.

E. THE ASYMPTOTIC SSE

In this subsection, the asymptotic SSE with the LAP density approaching infinity in a multi-UC scenario is derived and given in Corollary 2.

Corollary 2: When the LAP density becomes very large ($\lambda_L \rightarrow \infty$), the SSE converges to $\frac{\log(1+T_L)}{\pi R_L^2}$, where R_L is the sensing radius of an LAP, T_L is the LTE-LAA SINR threshold.

Proof: See Appendix F.

We can see that the asymptotic SSE increases with the LUE SINR threshold T_L and decrease with the LAP sensing radius R_L. This is because that the coverage probability of the LUE is close to 1 for an arbitrary finite threshold when the LAP density approaches infinity. This asymptotic SSE is only affected by the parameters in the LTE-LAA network,
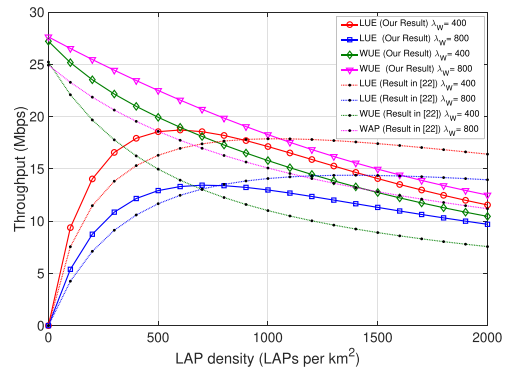

FIGURE 4. The LUE and WUE throughputs versus the LAP density for several WAP densities (400 and 800 WAPs per km²) with $M = 3$.

because the sum throughput provided by WAPs is negligible when the LAP density approaches infinity. The results in Corollary 2 can be used to provide design insights into how the deployment density of LAPs should be selected according to the number of available UCs, and can also be utilised to judge whether to deploy more LAPs in the current network from the point view of system.

IV. NUMERICAL RESULTS AND DISCUSSIONS

In this section, we present numerical results to show how the LUE and WUE throughputs, as well as the SSE, are affected by the LAP density and the number of UCs. Then we analyse the optimal LAP density obtained via our derived theoretical STP in (16), the STP LB of LUE in (28) and the results in [22]. Lastly, the fairness between the LUEs and the WUEs is analysed with respect to the LAP sensing region factor κ_L. The values of parameters used in the numerical results are listed in Table 2 unless otherwise specified. In this work, we set the SINR threshold as 5 dB without loss of generality, where a relative average UE throughput is achieved according to our simulation results.

A. UE THROUGHPUTS AND SSE ANALYSES

Fig. 4 illustrates both the LUE and WUE throughputs versus the LAP density for WAP densities being 400 and 800 WAPs per km² with three accessible UCs. The results show that, with the increase of LAP density, the WUE throughput decreases monotonically, while the LUE throughput increases with the LAP density under low LAP densities and decreases under high LAP densities. The increase in the LUE throughput is caused by the sharp enhancement of the coverage probability for the LUE. The main reason for the LUE-throughput degradation is that the coverage probability

$$\lambda_L^* = \arg\max_{\lambda_L}\left\{\frac{MN_{o,L}^{-1} + \frac{\Gamma(M+1,N_{o,L})}{N_{o,L}\Gamma(M+1,0)} + \frac{\Gamma(M+2,N_{o,L})}{\Gamma(M+2,0)} - \frac{(M+1)\Gamma(M+2,N_{o,L})}{N_{o,L}\Gamma(M+2,0)} - \frac{e^{-N_{o,L}}N_{o,L}^M}{\Gamma(M+2,0)}}{M + T_L^{\frac{2}{\alpha}}\left[sinc^{-1}(\frac{2\pi}{\alpha}) - {}_2F^1(1, \frac{2}{\alpha}; 1 + \frac{2}{\alpha}; -\frac{1}{T_L}) + \lambda_L^{-1}\lambda_W(\frac{P_W}{P_L})^{\frac{2}{\alpha}} sinc^{-1}(\frac{2\pi}{\alpha})\right]}\right\} \quad (18)$$

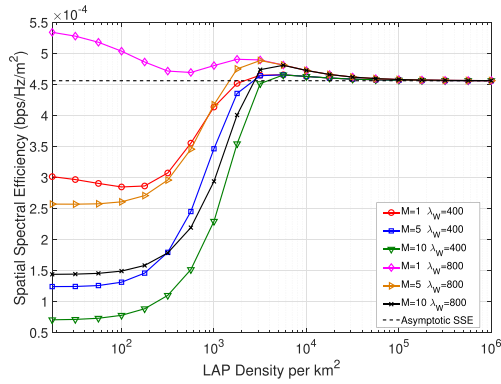**FIGURE 5.** The spatial spectral efficiency versus the LAP density.

FIGURE 6. The optimal LAP density for maximising the LUE throughput versus the UC number with WAP densities being 400 and 800 WAPs per km².

FIGURE 7. The optimal LUE throughput versus the number of UCs with WAP densities being 400 and 800 WAPs per km².

enhancement for the LUE is negligible under a high LAP density, while the MAP of the serving-AP decreases with the increase of LAP density. The LUE throughput curves also indicate that an optimal LAP density for maximising the LUE throughput exists. The LUE and WUE throughputs obtained based on [22] are also illustrated in this figure. We can see that the trend of the LUE throughput obtained based on [22] differs significantly with our derived results. This indicates that the results in [22] cannot be directly used to find the optimal LAP density for our system model using the CSMA/CA protocol. Moreover, as compared with the CLWNets using CSMA as the LBT mechanism for LAPs, the CLWNets using CSMA/CA has a higher successful transmission probability due to the lower chance of collision.

Fig. 5 illustrates the SSE versus the LAP density under WAP densities being 400 and 800 WAPs per km² with number of UCs being 1, 5 and 10. The asymptotic SSE is also plotted in this figure. The results validate the correctness of our derived asymptotic SSE. Moreover, for $M = 1$, and $\lambda_W = 400$ and 800, the deployment of low-density LAPs (under 100 LAPs per km²) reduces a bit of the SSE of the whole HetNet. For other cases of M and λ_W, with the increase of LAP density within the range of [10, 100] LAPs per km², the SSE does not change much. Furthermore, the SSE increases significantly when LAP density increases from 100 to 1, 250, and the SSEs with $\lambda_W = 1, 585$ WAPs per km² approach the asymptotic SSE. Therefore, the LAP density should be deployed around 1, 250 LAPs per km² to closely achieve the asymptotic SSE. In addition, interestingly, the SSE does not always improve with the increase of LAP density. The exception occurs when the number of UCs are in scarcity (e.g., $M = 1$, $\lambda_W = 800$), where the SSE decreases even if the LAP density approaches infinity. The main reason is that the sensing region of each LAP is larger than that of each WAP ($\kappa_L = 1.3$), then the asymptotic SSE as the WAP density approaching infinity is higher than that as the LAP density approaching infinity. When the number of UCs are in scarcity, the SSE has already become close to the asymptotic SSE as the WAP density approaching infinity, and the deployment of large number of LAPs can only achieve a lower asymptotic SSE.
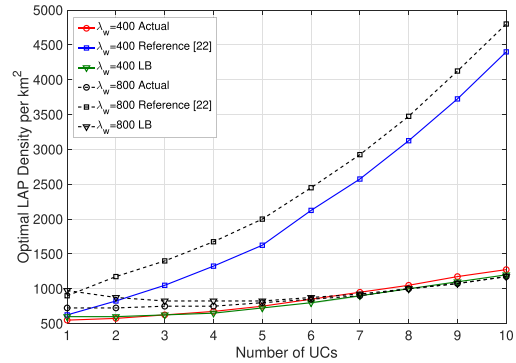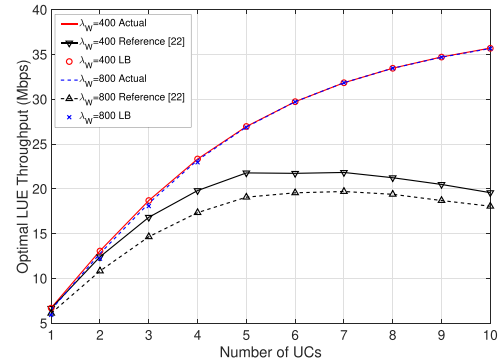
B. THE OPTIMAL LAP DENSITY
We analyse the optimal LAP density for maximising the LUE throughput in Fig. 6 based on our derived STP expression in (16), the STP LB of LUE in (28) and the results in [22]. We investigate the cases of λ_W being 400 and 800 WAPs per km² with the number of UCs ranging from 1 to 10. As our derived STP expressions have been validated by Monte Carlo simulations, the optimal LAP density obtained by the STP expression is called the actual optimal LAP density. The results show that the optimal LAP density obtained by the STP LB of LUE is close to the actual optimal LAP density, while a large gap occurs between the actual optimal LAP density and that obtained by the results in [22]. It indicates that the system model in [22] cannot be directly used in the analysis of the multi-UC HetNet using the CSMA/CA protocol, and our derived closed-form STP LB of LUE can be used to obtain a sufficiently accurate prediction of the optimal LAP density. This insight is further validated in Fig. 7, where we plot the maximised LUE throughput based on the optimal LAP densities in Fig. 6. We can see that the offset between the actual optimal LAP density and that obtained by the STP LB has negligible effect on the optimal LUE throughput, meanwhile our optimal LAP density leads to a much higher maximum LUE throughput than that obtained from [22], especially with a large number of actively accessible UCs. Furthermore, by incorporating the actual optimal LAP density in Fig. 6 into the SSE in Fig. 5, we can observe that, with
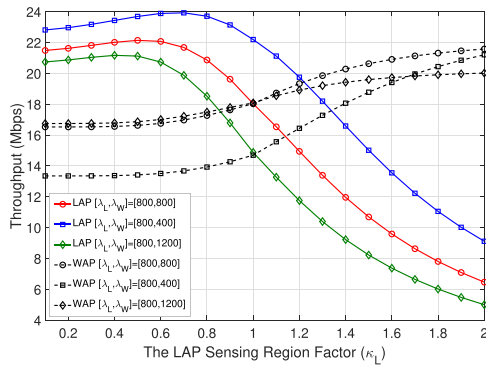
FIGURE 8. The LUE and WUE throughputs versus the LAP sensing region factor for several LAP and WAP densities with $M = 3$.

an increasing number of UCs, the SSE level with the optimal LAP density for maximising the LUE throughput increases and becomes more close to the asymptotic SSE. Therefore, the more number of actively accessible UCs are preferable in the multi-UC coexisting LTE-LAA and WiFi networks.

C. THE SENSING REGION OF LAPS
In Fig. 8, the fairness between the LUE and the WUE is analysed in terms of their throughputs against the LAP sensing region factor κ_L for several WAP densities and the LAP density of 800 LAPs per km^2. The fairness can be treated as the minimum throughput of the LUE and the WUE, and a better fairness means a larger minimum throughput. Firstly, the results show that LUE throughput increases when κ_L is smaller than 0.65. This trend has two causes: 1) When κ_L is smaller than 0.65, the MAP of an LAP is larger than 90%, where the variance of this MAP is limited. 2) When the MAP decreases, the aggregate interference suffered by the LUE is also decreased, which has a positive effect on the LUE throughput. As a result, when κ_L is smaller than 0.65, with an increase of κ_L, the effect of decreased aggregate interference on the LUE throughput outperforms that of the decreased MAP, thus the LAP curves show an increasing tendency. When κ_L is larger than 0.65, with the increase of κ_L, the decreased aggregate interference cannot compensate for the loss of LUE throughput caused by the decreased MAP, thus the LAP curves show a decreasing tendency. Secondly, the WUE throughput remain nearly constant when κ_L is smaller than 0.65. This is because the MAP of an LAP is larger than 90%, and the limited variance of MAP has a trivial effect on the WUE throughput. However, such a high MAP of the LAP will cause catastrophic degradation for the WUE throughput. As a result, the LUE throughput is much better than the WUE throughput, and the fairness between the LUE and the WUE is poor. Thirdly, the best fairness is achieved at $\kappa_L = 0.85$, 1, and 1.3 for WAP density of 400, 800, and 1200, respectively. This indicates that the fairness between the LUE and the WUE in terms of their throughputs can be improved by expanding the LAP sensing region if the LUE throughput outperforms the WUE throughput, but this will decrease the LUE throughput significantly.

V. CONCLUSION
In this work, we have developed analytical expressions for STPs for both LUEs and WUEs in the coexisting LTE-LAA and WiFi networks sharing multiple UCs, which are validated by the Monte Carlo simulation. Based on the STPs, the expressions of the UE throughput and the SSE have been obtained and we have analysed these performance metrics numerically versus the network density and the number of UCs. The results show that an optimal LAP density exists to maximise the LUE throughput in the multi-UC scenario, and our derived closed-form STP LB of LUE can be used to obtain a sufficiently accurate prediction of the optimal LAP density, When the LAP density is larger than 1, 585 LAPs per km^2, the SSE approaches the asymptotic SSE. Finally, with the optimal LAP density to maximise the LUE throughput, the greater number of actively accessible UCs are preferable because the SSE becomes closer to the asymptotic SSE. Nevertheless, the channel access priority of LAPs, which have effect on the MAPs of LAPs, are ignored and can be incorporated in the future work. In addition,there is still no performance analysis of the large-scale coexisting LTE-U and WiFi networks sharing multiple unlicensed channels, where LTE base stations use CSAT mechanism. The comparison between the LAA and LTE-U schemes in a large-scale coexisting network under the scenario of multiple UCs is another interesting topic to be done in the future.

APPENDIX A
PROOF OF LEMMA 1
According to Slivnyak's theorem [39], the tier-ξ AP can be positioned at origin without loss of generality because the position of AP belongs to a PPP. Based on the definition of the medium access indicators in (1), the MAP of the typical tier-ξ AP can be calculated as below:

$$\vartheta_\xi = \mathbb{P}(\mathcal{N}_o(R_\xi) < M) + \mathbb{P}(\mathcal{N}_o(R_\xi) \geq M)\mathbb{P}(t_o < \Delta(\mathcal{T}_o(R_\xi), M)). \tag{19}$$

The probability $\mathbb{P}(N(o, R_\xi) < M)$ can be calculated depended on the probability mass function of point number in a certain area for a PPP. The second term in the right hand side (r.h.s) of (19) indicates that the MAP when the number of neighbouring APs is larger than M. Because of the assumption of independent identically distributed back-off timer in each AP, the typical tier-ξ AP will be retained if the value of its back-off timer is among the lowest M ones of all the neighbouring APs plus itself. Consequently, the MAP ϑ_ξ can be transformed as follows:

$$\vartheta_\xi = \sum_{n=0}^{M-1} \frac{N_{o,\xi}^n \exp(-N_{o,\xi})}{n!} + \sum_{n=M}^{\infty} \frac{M}{n+1} \frac{N_{o,\xi}^n \exp(-N_{o,\xi})}{n!}$$
$$= e^{-N_{o,\xi}} \left[\sum_{n=0}^{M-1} \frac{N_{o,\xi}^n}{n!} + \frac{M}{N_{o,\xi}} \sum_{n=0}^{\infty} \frac{N_{o,\xi}^{n+1}}{(n+1)!} - \frac{M}{N_{o,\xi}} \sum_{n=0}^{M-1} \frac{N_{o,\xi}^{n+1}}{(n+1)!} \right] \tag{20}$$

The second step is obtained by adding and removing the summarization from 0 to $M-1$ of the second term after the first equals sign. According to the Taylor series expansion, the result in (20) can be transformed as:

$$\vartheta_\xi = \frac{e^{-N_{o,\xi}}}{N_{o,\xi}} \left[M(e^{N_{o,\xi}} - 1) - \sum_{n=1}^{M} \frac{(M-n)N_{o,\xi}^n}{n!} \right]. \quad (21)$$

By calculating the finite series $\nu = \sum_{n=1}^{M} \frac{(M-n)N_{o,\xi}^n}{n!}$ in Wolfram Mathematica, we have:

$$\nu = (M + 1 - N_{o,\xi}) \exp(-N_{o,\xi}) \frac{\Gamma(M+2, N_{o,\xi})}{\Gamma(M+2)}$$
$$- \exp(N_{o,\xi}) \frac{\Gamma(M+1, N_{o,\xi})}{\Gamma(M+1)} + \frac{N_{o,\xi}^{M+2}}{\Gamma(M+2)} - M. \quad (22)$$

By integrating (22) into (21), we can achieve the result in Lemma 1. A similar derivation can be found in [40] and we move a step further to obtain the MAP in closed form.

APPENDIX B
PROOF OF LEMMA 2
According to the assumption that a typical tier-ξ UE is always tagged to its closest tier-ξ AP, there will be no other tier-ξ APs in the ball of $\mathcal{B}(o, r_0^\xi)$. As a result, the MAP of this tier-ξ serving AP can be calculated based on the result in Lemma 1 by excluding the tier-ξ APs from the intersection region of $\mathcal{B}(o, r_0^\xi)$ and $\mathcal{B}(z_0^\xi, R_\xi)$, leading to the result in (7).

APPENDIX C
PROOF OF PROPOSITION 1
Without loss of generality, we give the derivation of the retaining probability of an interfering LAP $\mathbf{x}_i$. Due to the interfering LAP must use the same UC as the serving tier-ξ AP, the distance between them must be larger than the maximum radius of their sensing regions, i.e., $||\mathbf{x}_i - \mathbf{z}_0^\xi|| \geq \max\{R_L, R_\xi\}$, which can be denoted as $\mathbf{x}_i \in V_0^\xi(L)$. As a consequence, the retaining probability of the interfering LAP, which follows $\mathbf{x}_i \in \mathcal{B}(\mathbf{z}_0^\xi, \max\{R_L, R_\xi\})$, equals 0. Note that no other tier-ξ APs exist in $\mathcal{B}(o, r_0^\xi)$ because the serving tier-ξ AP is assumed as the nearest tier-ξ AP. Consequently, if the sensing region of the interfering LAP intersects with $\mathcal{B}(o, r_0^\xi)$, the expected number of interfering APs in this sensing region will be affected by the area of the intersection between $\mathcal{B}(o, r_0^\xi)$ and $\mathcal{B}(\mathbf{x}_i, R_L)$, which eventually influences the retaining probability of the interfering LAP. Accordingly, as illustrated in Fig. 9, the entire plane has been divided into three regions conditioned on that the serving AP is an LAP or a WAP. The outer region, i.e., $V_0^\xi(L) \cap V_1^\xi(L)$, represents no intersection occurs between $\mathcal{B}(o, r_0^\xi)$ and $\mathcal{B}(\mathbf{x}_i, R_L)$; The middle region, i.e., $V_0^\xi(L) \cap V_2^\xi(L)$, represents intersection occurs between $\mathcal{B}(o, r_0^\xi)$ and $\mathcal{B}(\mathbf{x}_i, R_L)$. Note that the interfering LAP cannot exist in $\mathcal{B}(o, r_0^\xi)$ when the serving AP is an LAP, thus $V_2^L(L)$ excludes this circle for the interfering LAPs, differing from $V_2^W(L)$; The inner region, which is the complementary of the two other regions, represents the
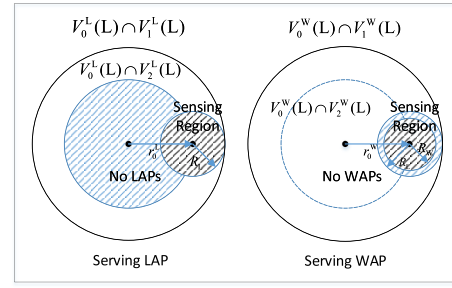

FIGURE 9. Illustration of the regions for interfering LAPs with serving LAP and WAP.

locations that interfering LAPs cannot occur. By assuming the retaining LAPs have equal probability (i.e., $1/M$) to access one of the M UCs, the retaining probability of an interfering LAP $\mathbf{x}_i$ can be achieved as the result in (12). The result for an interfering WAP can be obtained in a way similar to the interfering LAP, which is omitted in this work. It is worthy mentioning that this result is an approximation as we ignores the transmission state of APs in the intersection of $B(\mathbf{x}_i, R_L)$ and $B(\mathbf{x}_0, R_L)$. If some of these APs are granted transmission, the probability of the interfering AP being retained, which uses the same UC as the serving AP, increases because of less accessible UCs.

APPENDIX D
PROOF OF LEMMA 3
As the Palm coverage probability for a typical WUE can be obtained by some certain parameter exchanges in that of a typical LUE, thus we can focus on the derivation of a typical LUE. According to (9), the Palm coverage probability of a typical LUE can be transformed as

$$p_{\mathbf{x}_0}(r_0^L, \lambda_W, \lambda_L, T_L, M) = \mathbb{P}\left(\frac{P_L h_0^{\mathrm{LL}} l_L(||\mathbf{x}_0||)}{\widetilde{I}_{LL} + \widetilde{I}_{LW} + \sigma^2} > T_L | e_0^L = 1 \right). \quad (23)$$

By incorporating the definition of $\widetilde{I}_{LL}$ and $\widetilde{I}_{LW}$, we can transform the result above as follows:

$$e^{-\frac{\mu T_L \sigma^2}{P_L l_L(r_0^L)}} \mathbb{E}_{\widetilde{I}_{LW}} \left[e^{-\frac{\mu T_L}{l_L(r_0^L)} \frac{P_W}{P_L} \sum_{\mathbf{y}_j \in \Phi_W} h_j^{\mathrm{LW}} l_W(||\mathbf{y}_j||) e_{\mathbf{y}_j}^{LW} | e_0^L = 1} \right]$$
$$\times \mathbb{E}_{\widetilde{I}_{LL}} \left[e^{-\frac{\mu T_L}{l_L(r_0^L)} \sum_{\mathbf{x}_i \in \Phi_L \cap B^c(o, r_0^L)} h_i^{\mathrm{LL}} l_L(||\mathbf{x}_i||) e_{\mathbf{x}_i}^{LL} | e_0^L = 1} \right], \quad (24)$$

where $e_{\mathbf{x}_i}^{LL}$ and $e_{\mathbf{y}_j}^{LW}$ respectively denote the retaining indicators of the interfering LAP $\mathbf{x}_i$ and the interfering WAP $\mathbf{y}_j$, which equals 1 when the AP retains and equals 0 otherwise. Based on the retaining probability of the interfering LAP in (12), the expectation of the aggregate interference power $\widetilde{I}_{LL}$ generated by the retained interfering LAPs can be approximated as:

$$\mathbb{E}_{\widetilde{I}_{LL}} \left[e^{-\frac{\mu T_L}{l_L(r_0^L)} \sum_{\mathbf{x}_i \in \Phi_L \cap B^c(o, r_0^L)} h_i^{\mathrm{LL}} l_L(||\mathbf{x}_i||) e_{\mathbf{x}_i}^{LL} | e_0^L = 1} \right]$$
$$\approx e^{-\lambda_L \int_{\mathbb{R}^2/B(0, r_0^L)} \mathcal{R}_{LL}(x) \left\{ 1 - \mathbb{E}_{h_i^{LL}} \left[\exp(-h_i^{LL} \frac{\mu T_L}{l_L(r_0^L)} l_L(x)) \right] \right\} dx}, \quad (25)$$

which is obtained by the moment generating function for an inhomogeneous PPP [37]. By calculating the expectation of h_i^{LL}, we have:

$$\mathbb{E}_{\widetilde{I}_{LL}}\left[e^{-\frac{\mu T_L}{l_L(r_0^L)}\sum_{\mathbf{x}_i\in\Phi_L\cap B^c(o,r_0^L)}h_i^{LL}l_L(||\mathbf{x}_i||)e_{\mathbf{x}_i}^{LL}|e_0^L=1}\right]$$

$$= \exp\left(-\int_{\mathbb{R}^2/B(0,r)}\frac{\lambda_L\mathcal{R}_{LL}(x)}{1+\frac{l_L(r)}{T_L l_L(||x||)}}dx\right)$$

$$\stackrel{(a)}{=} \exp\left(-\int_0^{2\pi}\int_r^\infty\frac{\lambda_L\mathcal{R}_{LL}(\mathsf{p}(\rho,\theta))}{1+\frac{l_L(r)}{T_L l_L(\rho)}}\rho d\rho d\theta\right), \quad (26)$$

where step (a) is obtained by transforming an arbitrary point in the Cartesian coordinate system into the Polar coordinate system. Consequently, the expectation of the aggregate interference power $\widetilde{I}_{LL}$ is achieved. Similarly, the expectation of the aggregate interference power from WAPs can be obtained as follows:

$$\mathbb{E}\left[e^{-\frac{\mu T_L}{l_L(r_0^L)}\frac{P_W}{P_L}\sum_{\mathbf{y}_j\in\Phi_W}h_j^{LW}l_W(||\mathbf{y}_j||)\tilde{e}_{\mathbf{y}_j}^{LM}|\tilde{e}_0^L=1}\right]$$

$$= \exp\left(-\int_0^{2\pi}\int_0^\infty\frac{\lambda_W\mathcal{R}_{LW}(\mathsf{p}(\rho,\theta))}{1+\frac{P_L l_L(r_0^L)}{P_W T_L l_W(\rho)}}\rho d\rho d\theta\right). \quad (27)$$

Combining the results in (26) and (27), we can obtain the Palm coverage probability of the LUE. As aforementioned, the Palm coverage probability of a typical WUE can be obtained in a way similar as the LUE. Therefore, the final results in Lemma 3 have been yielded.

APPENDIX E
PROOF OF COROLLARY 1
According to Theorem 1, the STP of a typical LUE can be expressed as follows with $\sigma^2 = 0$:

$$\mathcal{P}_{st}^L(\lambda_W,\lambda_L,T_L,M)$$
$$\approx \mathbb{P}(e_0^L=1)\times\int_0^\infty\mathcal{L}_{\widetilde{I}_{LL}}\left(\frac{T_L}{l_L(r)}\right)\mathcal{L}_{\widetilde{I}_{LW}}\left(\frac{T_L}{l_L(r)}\right)f_{r_0^L}(r)dr, \quad (28)$$

where the functions $\mathcal{L}_{\widetilde{I}_{LL}}(\frac{T_L}{l_L(r)})$ and $\mathcal{L}_{\widetilde{I}_{LW}}(\frac{T_L}{l_L(r)})$ denote the Laplace transforms of the aggregate interference power from retained interfering LAPs and WAPs, respectively. Note that the value of function $\mathcal{A}(\cdot)$ is always smaller than $1/M$, then we have:

$$\mathcal{L}_{\widetilde{I}_{LL}}\left(\frac{T_L}{l_L(r)}\right) \geq \exp\left(-\int_0^{2\pi}\int_r^\infty\frac{\lambda_L/M}{1+\frac{l_L(r)}{T_L l_L(\rho)}}\rho d\rho d\theta\right). \quad (29)$$

According to [41], the expression in (30) can be translated into the following form as:

$$\mathcal{L}_{\widetilde{I}_{LL}}(\frac{T_L}{l_L(r)}) \geq e^{-\pi\frac{\lambda_L}{M}r^2 T_L^{\frac{2}{\alpha}}[sinc^{-1}(\frac{2\pi}{\alpha})-_2F^1(1,\frac{2}{\alpha};1+\frac{2}{\alpha};-\frac{1}{T_L})]}. \quad (30)$$

We denote the r.h.s of (30) as $\mathcal{H}_{LL}\left(\frac{T_L}{l_L(r)}\right)$. Similarly, the LB of $\mathcal{L}_{\widetilde{I}_{LW}}(\frac{T_L}{l_L(r)})$ can be obtained as:

$$\mathcal{L}_{\widetilde{I}_{LW}}\left(\frac{T_L}{l_L(r)}\right) \geq \exp\left(-\int_0^{2\pi}\int_0^\infty\frac{\lambda_W/M}{1+\frac{P_L l_L(r)}{P_W T_L l_W(\rho)}}\rho d\rho d\theta\right)$$

$$= e^{-\pi\frac{\lambda_W}{M}r^2\left(\frac{P_W}{P_L}T_L\right)^{\frac{2}{\alpha}}sinc^{-1}(\frac{2\pi}{\alpha})} \triangleq \mathcal{H}_{LW}\left(\frac{T_L}{l_L(r)}\right). \quad (31)$$

Addtionnally, as no LAPs can exist in the area closer than the serving LAP, the retaining probability of the serving LAP is larger than that of the typical LAP. Thus we have $\mathbb{P}(e_0^L=1) > \vartheta_L$. By incorporating this and the expressions in (30) and (31) into (28), we can achieve the LB of the STP for an LUE as the result in Corollary 1.

APPENDIX F
PROOF OF COROLLARY 2
By definition, the SSE Θ can be expressed by:

$$\Theta = \frac{1}{MB}\left[\lambda_L\mathcal{C}_L(\lambda_L,\lambda_W,T_L,M)+\lambda_W\mathcal{C}_W(\lambda_L,\lambda_W,T_L,M)\right]. \quad (32)$$

The first term on the r.h.s of (32) $\lambda_L\mathcal{C}_L(\lambda_L,\lambda_W,T_L,M)$ can be calculated as follows when $\lambda_L\to\infty$:

$$\lim_{\lambda_L\to\infty}\lambda_L\mathcal{C}_L(\lambda_L,\lambda_W,T_L,M) = B\log(1+T_L)\int_0^\infty\lim_{\lambda_L\to\infty}\lambda_L$$
$$\mathbb{P}(e_0^L=1|\mathbf{x}_0=(r,0))\mathbb{P}(\Psi_0^L>T_L|e_0^L=1,\mathbf{x}_0=(r,0))f_{r_0^L}(r)dr. \quad (33)$$

Note that $\lim_{\lambda_L\to\infty}f_{r_0^L}(r)$ equals $\delta(r)$, where $\delta(\cdot)$ is the Dirac delta function. On one hand, $f_{r_0^L}(r)$ is the serving-LAP-distance PDF function, we have $\int_0^\infty\lim_{\lambda_L\to\infty}f_{r_0^L}(r)dr = 1$. On the other hand, $f_{r_0^L}(r) = 2\pi\lambda_L r\exp(-\pi\lambda_L r^2)$, and $\lim_{\lambda_L\to\infty}2\pi\lambda_L r\exp(-\pi\lambda_L r^2)$ equals zero if $r > 0$. As a result, $\lim_{\lambda_L\to\infty}f_{r_0^L}(r)$ matches the property of the Dirac delta function. The term $\lim_{\lambda_L\to\infty}\lambda_L\mathbb{P}(e_0^L=1|\mathbf{x}_0=(r,0))$ in (33) can be transformed as follows:

$$\lim_{\lambda_L\to\infty}\lambda_L\mathbb{P}(e_0^L=1|\mathbf{x}_0=(r,0))$$
$$= \lim_{\lambda_L\to\infty}\lambda_L\mathcal{A}((\lambda_L+\lambda_W)\pi R_L^2-\lambda_L\mathcal{V}_{int}(r,R_L,r),M). \quad (34)$$

By denoting the term $(\lambda_L+\lambda_W)\pi R_L^2-\lambda_L\mathcal{V}_{int}(r,R_L,r)$ as $N_{o,L}'$, and combining with the expression of function $\mathcal{A}(\cdot)$ in (2), we have:

$$\lim_{\lambda_L\to\infty}\lambda_L\mathbb{P}(e_0^L=1|\mathbf{x}_0=(r,0)) = \lim_{\lambda_L\to\infty}\frac{\lambda_L}{N_{o,L}'}\left[\frac{\Gamma(M+1,N_{o,L}')}{\Gamma(M+1,0)}\right.$$
$$\left.+\frac{(N_{o,L}'-1-M)\Gamma(M+2,N_{o,L}')}{\Gamma(M+2,0)}-\frac{e^{-N_{o,L}'}N_{o,L}'^{M+1}}{\Gamma(M+2,0)}+M\right]. \quad (35)$$

We first note that $\lim_{\lambda_L \to \infty} \frac{N'_{o,L}}{\lambda_L} = \pi R_L^2 - \mathcal{V}_{int}(r, R_L, r)$. Then based on the property of the upper incomplete Gamma function $\Gamma(\hat{b}, a)$, we have $\lim_{\lambda_L \to \infty} \Gamma(\hat{b}, N'_{o,L}) = 0$. Moreover, according to Wolfram Mathematica, the function $\Gamma(\hat{b}, a)$ can be expanded as the following expression when $a \to \infty$:

$$\lim_{a \to \infty} \Gamma(\hat{b}, a) = \exp(-a) a^{\hat{b}} \left(\frac{1}{a} + \frac{\hat{b} - 1}{a^2} + O((\frac{1}{a})^3) \right). \quad (36)$$

Based on the L'Hospital's rule, we can have $\lim_{a \to \infty} a^{M+1} e^{-a} = 0$ and $\lim_{a \to \infty} a \Gamma(\hat{b}, a) = 0$. Therefore, the result in (35) can be obtained as $\frac{M}{\pi R_L^2 - \mathcal{V}_{int}(r, R_L, r)}$. After this, we derive the lower bound of the term $\lim_{\lambda_L \to \infty} \mathbb{P}\left(\Psi_0^L > T_L | \mathbf{e}_0^L = 1, \mathbf{x}_0 = (r, 0) \right)$, which can be expressed as follows based on (30) and (31) in the proof of Corollary 1:

$$\mathbb{P}\left(\Psi_0^L > T_L | \mathbf{e}_0^L = 1, \mathbf{x}_0 = (r, 0) \right) \geq \mathcal{H}_{LL}\left(\frac{T_L}{l_L(r)} \right) \mathcal{H}_{LW}\left(\frac{T_L}{l_L(r)} \right). \quad (37)$$

The upper bound of $\lim_{\lambda_L \to \infty} \mathbb{P}(\Psi_0^L > T_L | \mathbf{e}_0^L = 1, \mathbf{x}_0 = (r, 0))$ is 1. According to the property of the Dirac delta function, which satisfies $\int_0^\infty f(r) \delta(r) dr = f(0)$ where $f(\cdot)$ is an arbitrary continuous compactly supported function, the lower bound and upper bound of the term $\lim_{\lambda_L \to \infty} \lambda_L \mathcal{C}_L(\lambda_L, \lambda_W, T_L, M)$ are expressed as follows:

$$\frac{M}{\pi R_L^2} \leq \lim_{\lambda_L \to \infty} \lambda_L \mathcal{C}_L(\lambda_L, \lambda_W, T_L, M) \leq \frac{M}{\pi R_L^2}. \quad (38)$$

Due to the values of the upper and lower bounds are identical, the term $\lambda_L \mathcal{C}_L(\lambda_L, \lambda_W, T_L, M)$ converges to $\frac{M}{\pi R_L^2}$ with λ_L approaching infinity. On the other hand, the term $\lambda_W \mathcal{C}_W(\lambda_L, \lambda_W, T_L, M)$ equals 0 with λ_L approaching infinity because the MAP of a typical WAP and the coverage probability of its serving WUE are both close to 0. Consequently, the SSE converges to $\frac{\log(1+T_L)}{\pi R_L^2}$.

REFERENCES

[1] *Global Mobile Data Traffic Forecast Update, 2016–2021*, Cisco Vis. Netw. Index, San Jose, CA, USA, 2017.

[2] Q. C. Li, H. Niu, A. T. Papathanassiou, and G. Wu, "5G network capacity: Key elements and technologies," *IEEE Veh. Technol. Mag.*, vol. 9, no. 1, pp. 71–78, Mar. 2014.

[3] H. Zhang, X. Chu, W. Guo, and S. Wang, "Coexistence of Wi-Fi and heterogeneous small cell networks sharing unlicensed spectrum," *IEEE Commun. Mag.*, vol. 53, no. 3, pp. 158–164, Mar. 2015.

[4] Y. Wu, W. Guo, H. Yuan, L. Li, S. Wang, X. Chu, and J. Zhang, "Device-to-device meets LTE-unlicensed," *IEEE Commun. Mag.*, vol. 54, no. 5, pp. 154–159, May 2016.

[5] *Extending LTE Advanced to Unlicensed Spectrum, White Paper*, Qualcomm, San Diego, CA, USA, Dec. 2013.

[6] H.-J. Kwon, J. Jeon, A. Bhorkar, Q. Ye, H. Harada, Y. Jiang, L. Liu, S. Nagata, B. L. Ng, T. Novlan, J. Oh, and W. Yi, "Licensed-assisted access to unlicensed spectrum in LTE release 13," *IEEE Commun. Mag.*, vol. 55, no. 2, pp. 201–207, Feb. 2017.

[7] *Study on NR-Based Access to Unlicensed Spectrum (Release 16)*, document TR 38.889 V1.0.0, 3GPP, Nov. 2018.

[8] F. Liu, E. Bala, E. Erkip, M. C. Beluri, and R. Yang, "Small-cell traffic balancing over licensed and unlicensed bands," *IEEE Trans. Veh. Technol.*, vol. 64, no. 12, pp. 5850–5865, Dec. 2015.

[9] C. Cano and D. J. Leith, "Unlicensed LTE/WiFi coexistence: Is LBT inherently fairer than CSAT?" in *Proc. IEEE Int. Conf. Commun. (ICC)*, Kuala Lumpur, Malaysia, May 2016, pp. 1–6.

[10] H. Ko, J. Lee, and S. Pack, "A fair listen-before-talk algorithm for coexistence of LTE-U and WLAN," *IEEE Trans. Veh. Technol.*, vol. 65, no. 12, pp. 10116–10120, Dec. 2016.

[11] F. Liu, E. Bala, E. Erkip, M. C. Beluri, and R. Yang, "Small-cell traffic balancing over licensed and unlicensed bands," *IEEE Trans. Veh. Technol.*, vol. 64, no. 12, pp. 5850–5865, Dec. 2015.

[12] N. Bitar, M. O. A. Kalaa, S. J. Seidman, and H. H. Refai, "On the coexistence of LTE-LAA in the unlicensed band: Modeling and performance analysis," *IEEE Access*, vol. 6, pp. 52668–52681, 2018.

[13] J. Yi, W. Sun, S. Park, and S. Choi, "Performance analysis of LTE-LAA network," *IEEE Commun. Lett.*, vol. 22, no. 6, pp. 1236–1239, Jun. 2018.

[14] Z. Fu, W. Xu, Z. Feng, X. Lin, and J. Lin, "Throughput analysis of LTE-licensed-assisted access networks with imperfect spectrum sensing," in *Proc. IEEE Wireless Commun. Netw. Conf. (WCNC)*, San Francisco, CA, USA, Mar. 2017, pp. 1–6.

[15] H. Lee, H. Kim, H. J. Yang, J. T. Kim, and S. Baek, "Performance analysis of license assisted access LTE with asymmetric hidden terminals," *IEEE Trans. Mobile Comput.*, vol. 17, no. 9, pp. 2141–2154, Sep. 2018.

[16] Y. Li, F. Baccelli, J. G. Andrews, T. D. Novlan, and J. C. Zhang, "Modeling and analyzing the coexistence of Wi-Fi and LTE in unlicensed spectrum," *IEEE Trans. Wireless Commun.*, vol. 15, no. 9, pp. 6310–6326, Sep. 2016.

[17] X. Wang, T. Q. S. Quek, M. Sheng, and J. Li, "Throughput and fairness analysis of Wi-Fi and LTE-U in unlicensed band," *IEEE J. Sel. Areas Commun.*, vol. 35, no. 1, pp. 63–78, Jan. 2017.

[18] Y. Li, F. Baccelli, J. G. Andrews, T. D. Novlan, and J. C. Zhang, "Modeling and analyzing the coexistence of Wi-Fi and LTE in unlicensed spectrum," *IEEE Trans. Wireless Commun.*, vol. 15, no. 9, pp. 6310–6326, Sep. 2016.

[19] R. Yin, G. Yu, A. Maaref, and G. Y. Li, "LBT-based adaptive channel access for LTE-U systems," *IEEE Trans. Wireless Commun.*, vol. 15, no. 10, pp. 6585–6597, Oct. 2016.

[20] H. Ko, J. Lee, and S. Pack, "Joint optimization of channel selection and frame scheduling for coexistence of LTE and WLAN," *IEEE Trans. Veh. Technol.*, vol. 67, no. 7, pp. 6481–6491, Jul. 2018.

[21] R. Yin, Y. Zhang, F. Dong, A. Wang, and C. Yuen, "Energy efficiency optimization in LTE-U based small cell networks," *IEEE Trans. Veh. Technol.*, vol. 68, no. 2, pp. 1963–1967, Feb. 2019.

[22] X. Ding, C.-H. Liu, L.-C. Wang, and X. Zhao, "Coexisting success probability and throughput of multi-RAT wireless networks with unlicensed band access," *IEEE Wireless Commun. Lett.*, vol. 5, no. 1, pp. 4–7, Feb. 2016.

[23] A. K. Bairagi, N. H. Tran, W. Saad, Z. Han, and C. S. Hong, "A game-theoretic approach for fair coexistence between LTE-U and Wi-Fi systems," *IEEE Trans. Veh. Technol.*, vol. 68, no. 1, pp. 442–455, Jan. 2019.

[24] Q. Wei, L. Wang, Z. Feng, and Z. Ding, "Wireless resource management in LTE-U driven heterogeneous V2X communication networks," *IEEE Trans. Veh. Technol.*, vol. 67, no. 8, pp. 7508–7522, Aug. 2018.

[25] Z. Yao, W. Cheng, and H. Zhang, "Full-duplex assisted LTE-U/Wifi coexisting networks in unlicensed spectrum," *IEEE Access*, vol. 6, pp. 40085–40095, 2018.

[26] H. S. Dhillon, R. K. Ganti, F. Baccelli, and J. G. Andrews, "Modeling and analysis of K-tier downlink heterogeneous cellular networks," *IEEE J. Sel. Areas Commun.*, vol. 30, no. 3, pp. 550–560, Apr. 2012.

[27] J. G. Andrews, F. Baccelli, and R. K. Ganti, "A tractable approach to coverage and rate in cellular networks," *IEEE Trans. Commun.*, vol. 59, no. 11, pp. 3122–3134, Nov. 2011.

[28] T. S. Rappaport, *Wireless Communications: Principles and Practice*. Upper Saddle River, NJ, USA: Prentice-Hall, 1996.

[29] T. S. Rappaport, *IEEE Standard for Information Technology—Telecommunications and Information Exchange Between Systems Local and Metropolitan Area Networks—Specific Requirements—Part 11: Wireless LAN Medium Access Control (MAC) and Physical Layer (PHY) Specifications*, IEEE Standard 802.11-2016, Dec. 2016, pp. 1–3534.

[30] G. Yuan, X. Zhang, W. Wang, and Y. Yang, "Carrier aggregation for LTE-advanced mobile communication systems," *IEEE Commun. Mag.*, vol. 48, no. 2, pp. 88–93, Jan. 2010.

[31] *Harmonized European Standard; Broadband Radio Access Networks (BRAN); 5 GHz High Performance RLAN*, document ETSI EN 301 893, V2.1.1, 2017.

[32] *Study on Licensed-Assisted Access to Unlicensed Spectrum*, document 3GPP TR 36.889, V2.1.1, 2017.

[33] T. Zhang, J. Zhao, L. An, and D. Liu, "Energy efficiency of base station deployment in ultra dense HetNets: A stochastic geometry analysis," *IEEE Wireless Commun. Lett.*, vol. 5, no. 2, pp. 184–187, Apr. 2016.

[34] Y. Zhong, W. Zhang, and M. Haenggi, "Stochastic analysis of the mean interference for the RTS/CTS mechanism," in *Proc. IEEE Int. Conf. Commun. (ICC)*, Jun. 2014, pp. 1996–2001.

[35] A. Mbengue and Y. Chang, "Performance analysis of LAA/Wi-Fi coexistence: Stochastic geometry model," in *Proc. IEEE Wireless Commun. Netw. Conf. (WCNC)*, Apr. 2018, pp. 1–6.

[36] H. Kwon, S. Kim, and B. G. Lee, "Opportunistic multi-channel CSMA protocol for OFDMA systems," *IEEE Trans. Wireless Commun.*, vol. 9, no. 5, pp. 1552–1557, May 2010.

[37] H. Q. Nguyen, F. Baccelli, and D. Kofman, "A stochastic geometry analysis of dense IEEE 802.11 networks," in *Proc. IEEE INFOCOM-26th IEEE Int. Conf. Comput. Commun.*, May 2007, pp. 1199–1207.

[38] Z. Lin, Y. Li, S. Wen, Y. Gao, X. Zhang, and D. Yang, "Stochastic geometry analysis of achievable transmission capacity for relay-assisted device-to-device networks," in *Proc. IEEE Int. Conf. Commun. (ICC)*, Sydney, NSW, Australia, May 2014, pp. 2251–2256.

[39] F. Baccelli and B. Błaszczyszyn, "Stochastic geometry and wireless networks: Volume II applications," *Found. Trends Netw.*, vol. 4, nos. 1–2, pp. 1–312, 2010.

[40] H. ElSawy, E. Hossain, and S. Camorlinga, "Multi-channel design for random CSMA wireless networks: A stochastic geometry approach," in *Proc. IEEE Int. Conf. Commun. (ICC)*, Jun. 2013, pp. 1656–1660.

[41] H. Hu, J. Weng, and J. Zhang, "Coverage performance analysis of FeICIC low-power subframes," *IEEE Trans. Wireless Commun.*, vol. 15, no. 8, pp. 5603–5614, Aug. 2016.

XIAOLI CHU (M'06–SM'15) received the B.Eng. degree in electronic and information engineering from Xi'an Jiaotong University, in 2001, and the Ph.D. degree in electrical and electronic engineering from the Hong Kong University of Science and Technology, in 2005. From 2005 to 2012, she was with the Centre for Telecommunications Research, King's College London. She is currently a Reader with the Department of Electronic and Electrical Engineering, The University of Sheffield, U.K. She has coauthored over 140 peer-reviewed journal and conference papers. She is the lead editor/author of *Heterogeneous Cellular Networks: Theory, Simulation and Deployment* (Cambridge University Press) and *4G Femtocells: Resource Allocation and Interference Management* (Springer). She was a co-recipient of the IEEE Communications Society 2017 Young Author Best Paper Award. She received the IEEE Communications Letters Editor Award, in 2018. She was the Co-Chair of the Wireless Communications Symposium for the IEEE International Conference on Communications (ICC) 2015 and has organized six workshops on heterogeneous and small cell networks for IEEE ICC, GLOBECOM, WCNC, and PIMRC. She is also an Editor of the IEEE COMMUNICATIONS LETTERS and the IEEE WIRELESS COMMUNICATIONS LETTERS. She was a Guest Editor of the IEEE TRANSACTIONS ON VEHICULAR TECHNOLOGY and the *Journal of Mobile Networks and Applications* (ACM/Springer).
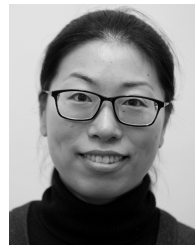
HAONAN HU received the B.S. degree from the Beijing University of Posts and Telecommunications, China, in 2010, the M.S. degree from the Chongqing University of Posts and Telecommunications, China, in 2013, and the Ph.D. degree from the Department of Electronic and Electrical Engineering, The University of Sheffield, U.K., in 2019. He is currently a Lecturer with the Chongqing University of Posts and Telecommunications. His research interests include interference management, heterogeneous networks, Fog-RAN, LTE-U networks, and stochastic geometry.

QIANBIN CHEN received the B.Sc. degree in radio electronics from Sichuan University, Chengdu, China, in 1988, the M.E. degree in signal and information processing from the Chongqing University of Posts and Telecommunications (CQUPT), Chongqing, China, in 1995, and the Ph.D. degree in communication and information system from the University of Electronic Science and Technology of China (UESTC), Chengdu, in 2002. He is currently a Professor with the School of Communication and Information Engineering, CQUPT, and the Director of the Chongqing Key Lab of Mobile Communications Technology. He has published over 200 articles in journals and peer-reviewed conference proceedings and has coauthored seven books. He holds 98 granted national patents. He is also a Fellow of the China Institute of Communications (CIC).

YUAN GAO received the B.S. degree from the Beijing University of Posts and Telecommunications, in 2013, and the M.S. degree from the Imperial College, in 2014. He is currently pursuing the Ph.D. degree with the University of Sheffield, in 2020. He is also a Wireless Engineer with Ranplan Wireless Ltd. His research interests include LTE-U, NR-U, machine learning, optimization, and resource allocation.

JIE ZHANG is the Founder and the Chief Scientific Officer (CSO) of Ranplan Wireless, a public company listed on Nasdaq OMX. He has been the Chair in Wireless Systems with the Department of Electronic and Electrical Engineering, The University of Sheffield, since January 2011. Along with his students and colleagues, he has pioneered research in small cell and heterogeneous network (HetNet) and published some of the landmark articles and book on these topics, widely used by both academia and industry. With Google scholar citations in excess of 6300, he is a renowned authority in his field of expertise. In his current roles as CSO at Ranplan and a Chair Professor at Sheffield University, he leads a team of over 30 researchers at Ph.D. candidate level or above. The team has 12 ongoing research projects funded by the European Commission and Innovate U.K. on data-driven proactive network optimization, millimeter-wave small cell communications in the built environments, and modeling and design of smart environments. Prior to his current appointments, he studied and worked at Imperial College London, Oxford University, and the University of Bedfordshire, reaching the rank of a Lecturer, a Reader, and a Professor, in 2002, 2005, and 2006, respectively.

JILIANG ZHANG (M'15–SM'19) received the B.S., M.S., and Ph.D. degrees from the Harbin Institute of Technology, in 2007, 2009, and 2014, respectively. He is currently a Marie Curie Research Fellow with the Department of Electronic and Electrical Engineering, The University of Sheffield, Sheffield, U.K. His research interests include stochastic geometry, neural networks, MIMO channel measurement and modeling, single-RF MIMO systems, and relay systems.

• • •